International Journal of Multiphase Flow 36 (2010) 202–209

Contents lists available at ScienceDirect

International Journal of Multiphase Flow

journal homepage: www.elsevier.com/locate/ijmulflow

A method for direct simulation of flexible fiber suspensions using lattice Boltzmann equation with external boundary force

Jingshu Wu, Cyrus K. Aidun *

G. W. Woodruff School of Mechanical Engineering, Georgia Institute of Technology, 500 10th Street NW, Atlanta, GA 30332, USA

ARTICLE INFO

Article history:
Received 14 July 2009
Received in revised form 4 November 2009
Accepted 5 November 2009
Available online 10 November 2009

Keywords:
Flexible fiber
Lattice Boltzmann
Numerical simulation

ABSTRACT

The computational method presented here can be used to study the effect of volume fraction and particle deformation on the rheology and microstructure of deformable fibers suspended in Newtonian fluid. In this method, the flow is computed on a fixed regular 'lattice' using the lattice Boltzmann method, where each solid particle is mapped onto a Lagrangian frame moving continuously through the domain. Instead of the standard bounce-back method, an external boundary force is used to impose the no-slip boundary condition at the fluid–solid interface for stationary or moving boundaries. The motion and orientation of the fiber are obtained from Newtonian dynamics equations. Although the external boundary force method is general, in this application it is used in conjunction with a flexible fiber model, which calculates the flexible fiber deformation by the real material properties. The methodology is validated by comparing with experimental and theoretical results.

1. Introduction

Newtonian fluid with suspensions usually shows complex non-Newtonian flow characteristics. In some situations, the particles are deformable and make problems even more complicated. Treating these suspensions as rigid particles ignores important physical behavior. For example, the effective viscosity of actual fiber suspension is 7–13% larger than the equivalent rigid fiber suspension (Forgacs and Mason, 1959; Blakeney, 1966; Goto et al., 1986). Understanding the underlying physical processes is very important in simulation and optimization of engineering applications. Experimental techniques are also critical for understanding the basic mechanism, but they have certain drawbacks in these situations. It is difficult to measure the shape and deformation of deformable particles and rheological quantities such as self-diffusivities in experiments.

Investigating the rheology of particle suspensions, Einstein (1906) argued that for a dilute suspension of spheres, the energy dissipation should be balanced by the work done by the motion of the suspended particle, and the relative viscosity is a function of the volume concentration. Based on this theory, Jeffery (1922) developed a model for an ellipsoid in a Newtonian fluid. He calculated the stress and the shear viscosity for the dilute suspension. The Brownian motion gives random deviation from Jeffery's result. Hinch and Leal (1972) described the Brownian motion by a diffusion term in the equation of fiber orientation and studied the effect of the Brownian motion on the rheology of dilute fiber suspensions. Lee and Springer (1982) introduced a two-body interaction term into Jeffery's equation of motion and thus showed how the fiber–fiber interactions affect the fiber orientation distribution.

Anczurowski and Mason (1967) and Okagawa and Mason (1973) have shown that Jeffery's results will not hold in semi-dilute and concentrated regimes. Batchelor (1970, 1971) derived a general constitutive equation for suspensions in a Newtonian fluid and calculated the stress field of a concentrated elongated particle suspension. Doi and Edwards (1978a,b) proposed a scheme to extend the results from dilute theory to higher volume concentration. Dinh and Armstrong (1984) discussed the dynamics of non-Brownian fiber suspensions using an effective medium approximation and derived a constitutive equation that includes fiber–fiber interaction and describes the rheological behavior in the semi-concentrated regime. Folgar and Tucker (1984) studied the fiber orientation distribution in a semi-concentrated suspension. They added a dispersion term which is structured like a Brownian motion force in Jeffery's equation to model the fiber–fiber interaction. Shaqfeh and Koch (1988, 1990) defined a diagrammatic expansion to describe the hydrodynamic interactions that cause the deviation from the Jeffery's orbit. Stover et al. (1992) experimentally measured the orientations of fibers in a semi-dilute suspension in a cylindrical Couette device and examined the existing theories. Claeys and Brady (1993) have done extensive numerical calculations for elongated particles in an unbounded fluid with hydrodynamic interactions using Stokesian dynamics.

In all the above mentioned works, the fiber is considered as a rigid rod-like cylinder in Stokes flow where inertia of fluid and fiber is ignored. These assumptions allow one to develop theories about the fiber suspension without the complication of fiber

* Corresponding author. Tel.: +1 404 894 6645; fax: +1 404 894 0364.
E-mail address: cyrus.aidun@me.gatech.edu (C.K. Aidun).

0301-9322/$ - see front matter © 2009 Elsevier Ltd. All rights reserved.
doi:10.1016/j.ijmultiphaseflow.2009.11.003

deformation. But it is well known that the fiber shape has an important effect on suspension microstructure and rheology. Experimental studies (Forgacs and Mason, 1959; Blakeney, 1966; Goto et al., 1986) have shown that slight fiber curvature would change the period of fiber rotation, the drag on the fiber and the shear viscosity of the suspension. Simulations of flexible fibers, composed of spring linked spheres (Yamamoto and Matsuoka, 1992; Joung et al., 2001) and spheroids (Ross and Klingenberg, 1997; Qi, 2006) have successfully reproduced single fiber motions and predicted suspension viscosities. Schmid et al. (2000) and Lindstrom and Uesaka (2008) did similar investigations by using a "chain of rods" model to simulate a flexible fiber with high aspect ratio.

In this study, we use the lattice Boltzmann method (LBM) with external boundary force (EBF) (Wu and Aidun, 2009) to simulate and obtain the microstructure and rheological properties in flexible fiber suspensions at particle-level. The flow is computed on a fixed regular 'lattice' using the lattice Boltzmann method, where the fiber is mapped onto a Lagrangian frame moving continuously through the domain. An efficient flexible fiber model has been developed to simulate fibers with high aspect ratio. The lattice Boltzmann method for analysis of fluid flow problems (Chen et al., 1992; Hou et al., 1995; Mcnamara and Zanetti, 1988) has been extended to direct simulation of particles suspended in fluid (Ladd, 1994; Aidun and Lu, 1995; Aidun et al., 1998). In these methods, the no-slip boundary condition at the fluid–solid interface is based on the standard "bounce-back" (SBB) rule. The interaction boundary is represented at the mid-points of the links which are cut by the solid particle boundary. A fluid–solid collision function is used to account for the momentum exchange and apply the interaction force to both fluid and the particle. With LBM–SBB method, the solid boundary (broken line in Fig. 1a) will not move continuously and smoothly in space; instead it will jump from one midpoint to another causing fluctuations. To reduce this fluctuation, one can use a finer lattice grid with more nodes at the boundary increasing the computational time, or higher order bounce back based on interpolations. Although the interpolated bounce-back (IBB) methods (Bouzidi et al., 2001; Ginzburg and d'Humieres, 2003) are more accurate compare to SBB, in addition to being computationally expensive, they require at least two or three fluid nodes between nearby solid surfaces for interpolation. This excludes application to non-dilute suspensions of solid particles with close interaction between the particles or the particle and the boundary (Chun and Ladd, 2007; Ding and Aidun, 2003). To reach a stable and accurate result in existing LBM–SBB methods, the diameter of the fiber, D, must be about 4–10 times the unit lattice size, Δx^{LBM} (Qi, 2006; Rezak, 2008). While in LBM–EBF method, D is about 0.4 to 1 times Δx^{LBM}. This advantage makes EBF more efficient compared to SBB method in fiber simulation. For example, to simulate a fiber suspension with aspect ratio $r_p = 20$, in LBM–SBB method, the fiber length $L = 80$, and in order to eliminate the wall effect, the length of the fluid domain has to be at least five times the fiber length, that is $400 \times 400 \times 400$. But in LBM–EBF method, the corresponding fiber length $L = 8$ and the domain size is $40 \times 40 \times 40$.

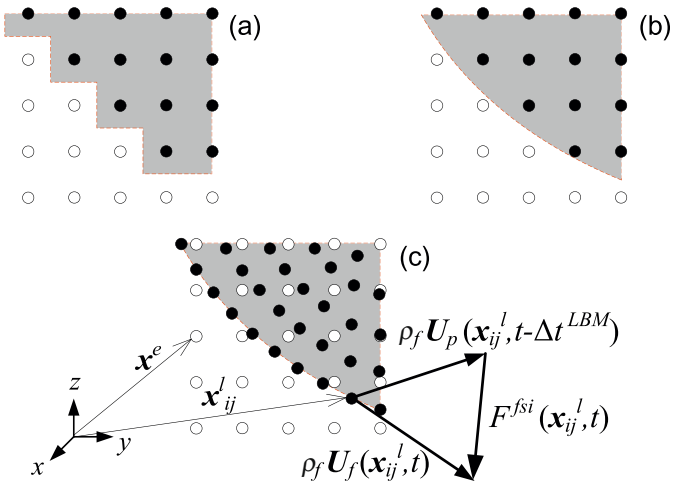

Fig. 1. (a) Regular Eulerian grid for standard bounce-back (SBB) rule. (b) Regular Eulerian grid for Interpolated bounce-back (IBB) rule. In (a) the filled circles (•) are the fluid nodes covered by the solid, open circles (○) are the fluid nodes outside the solid particle. (c) The solid Lagrangian nodes (•) and fluid Eulerian nodes (○) for external boundary force (EBF) method. The red broken line (···) shows the solid boundary. Note that the solid boundary nodes in (c) are located exactly on the fluid–solid boundary Γ.

The remaining part of this paper is organized as follows. In Section 2, the LBM–EBF method and the flexible fiber model are described in detail covering the basics of the fluid–solid interaction including a summary of the basic steps. Several sample simulations with rigid and flexible fiber suspensions are presented and compared with theoretical solutions and experimental results in Section 3 to validate the accuracy of the new method. We close the paper with some concluding remarks in Section 4.

2. Methodology

2.1. Fluid–solid interaction

The presence of an external *body* force in the kinetic-based conservation equations has been discussed in classical kinetic theory (Liboff, 2003). The connection between the source term in the LBE and the resulting *body* force field in the Navier–Stokes equation has also been discussed since the inception of the LBM two decades ago (Buick and Greated, 2000; Guo et al., 2002; He et al., 1997; Ladd and Verberg, 2001; Martys et al., 1998). A method based on an external *boundary* force (Goldstein et al., 1993) at the fluid–solid interface in the Navier–Stokes equation applied to the LBM (Wu and Aidun, 2009) to implement the no-slip boundary condition for simulation of flexible fiber is presented here. The LBM–EBF method does not have the 'Galilean Invariance' error associated with the SBB method as outlined by Clausen and Aidun (2009).

To present the LBM–EBF equations, the solid and fluid domains are defined as Π_s and Π_f respectively, with solid–fluid boundary, Γ. There are N and M discrete solid and fluid nodes in the set of discrete solid and fluid position vectors, Π_s^N and Π_f^M, respectively. The subset of boundary nodes for the solid and fluid domain are defined as Γ_s and Γ_f. The position vector in terms of unit vectors $\boldsymbol{e_x}$, $\boldsymbol{e_y}$, and $\boldsymbol{e_z}$ in the fixed Cartesian coordinate system is given by $\boldsymbol{x} = x\boldsymbol{e_x} + y\boldsymbol{e_y} + z\boldsymbol{e_z}$.

The discrete position vector for the jth node on ith particle is defined as $\boldsymbol{x}_{ij}^{l} \in \Pi_s^N$, and the position vector for the fluid nodes is defined as $\boldsymbol{x}^e \in \Pi_f^M$, where superscripts l and e denote solid nodes and fluid nodes, respectively. On the solid and the fluid points $\boldsymbol{x}$ on Γ at time, t, the force per unit volume acting on the solid $\boldsymbol{F}^{fsi}(\boldsymbol{x}, t)$ is equal to the force per unit volume acting on the fluid $\boldsymbol{g}(\boldsymbol{x}, t)$; that is, $\boldsymbol{F}^{fsi}(\boldsymbol{x}, t) = -\boldsymbol{g}(\boldsymbol{x}, t)$ for $\boldsymbol{x} \in \Gamma$. The Navier–Stokes and continuity equations with the external boundary force can be written as

$$\left.\begin{aligned} \rho\left(\tfrac{\partial \boldsymbol{u}}{\partial t} + \boldsymbol{u}\cdot\nabla\boldsymbol{u}\right) &= -\nabla P + \mu\nabla^2\boldsymbol{u} + \boldsymbol{g}(\boldsymbol{x}, t), \\ \nabla\cdot\boldsymbol{u} &= 0, \end{aligned}\right\} \tag{1}$$

where $\boldsymbol{x} \in \Pi_f$. In this equation, $\boldsymbol{g}(\boldsymbol{x}, t) = 0$ when $\boldsymbol{x} \notin \Gamma$. In the discretized formulation, the external boundary force, $\boldsymbol{g}$, is evaluated on the fluid boundary node as shown below (Eq. (5)).

Usually the boundary nodes will not coincide with the fluid nodes, so the fluid velocity $\boldsymbol{U}_f\left(\boldsymbol{x}_{ij}^l,t\right)$ at solid boundary node $\boldsymbol{x}_{ij}^l$ at time t should be evaluated by

$$\boldsymbol{U}_f(\boldsymbol{x}_{ij}^l,t)=\int_{\Pi_f^M}\boldsymbol{u}(\boldsymbol{x}^e,t)D\left(\boldsymbol{x}^e-\boldsymbol{x}_{ij}^l\right)\mathrm{d}\boldsymbol{x}^e,\quad \boldsymbol{x}_{ij}^l\in\Gamma_s, \tag{2}$$

where $D(\boldsymbol{x}^e-\boldsymbol{x}_{ij}^l)$ is a discrete Dirac delta function in three-dimensional domain (Peskin, 2002).

The initial velocity, position and orientation of fiber and the initial conditions of the suspending fluid are known. Due to no-slip boundary condition, the fluid velocity at the particle boundary is equal to the particle velocity, that is

$$\boldsymbol{U}_f\left(\boldsymbol{x}_{ij}^l,t-\Delta t^{LBM}\right)=\boldsymbol{U}_p\left(\boldsymbol{x}_{ij}^l,t-\Delta t^{LBM}\right), \tag{3}$$

where the LBM time step $\Delta t^{LBM}=1$, $\boldsymbol{U}_p\left(\boldsymbol{x}_{ij}^l,t-\Delta t^{LBM}\right)$ is the particle velocity at solid boundary node $\boldsymbol{x}_{ij}^l$ at the previous time step. The fluid–solid interaction force per unit volume acting on the solid boundary node $\boldsymbol{F}^{fsi}\left(\boldsymbol{x}_{ij}^l,t\right)$ is given by

$$\boldsymbol{F}^{fsi}(\boldsymbol{x}_{ij}^l,t)=\rho_f\left(\boldsymbol{U}_f\left(\boldsymbol{x}_{ij}^l,t\right)-\boldsymbol{U}_p\left(\boldsymbol{x}_{ij}^l,t-\Delta t^{LBM}\right)\right)\Big/\Delta t^{LBM},\quad \boldsymbol{x}_{ij}^l\in\Gamma_s, \tag{4}$$

where ρ_f is the density of the fluid. The resulting force acting on the fluid boundary nodes is given by

$$\boldsymbol{g}(\boldsymbol{x}^e,t)=-\int_{\Gamma_s}\boldsymbol{F}^{fsi}\left(\boldsymbol{x}_{ij}^l,t\right)D\left(\boldsymbol{x}^e-\boldsymbol{x}_{ij}^l\right)\mathrm{d}\boldsymbol{x}_{ij}^l,\quad \boldsymbol{x}^e\in\Gamma_f, \tag{5}$$

where $\boldsymbol{g}$ will be used as an external boundary force term in the LB equation as will be discussed in Section 2.2.

$\boldsymbol{F}\left(\boldsymbol{x}_{ij}^l,t\right)$ is the combination of the fluid–solid interaction force $\boldsymbol{F}^{fsi}\left(\boldsymbol{x}_{ij}^l,t\right)$ and the external force $\boldsymbol{F}^{ext}\left(\boldsymbol{x}_{ij}^l,t\right)$ which could include the gravitational force, interparticle (electrical or lubrication) forces; therefore,

$$\boldsymbol{F}\left(\boldsymbol{x}_{ij}^l,t\right)=\boldsymbol{F}^{fsi}\left(\boldsymbol{x}_{ij}^l,t\right)+\boldsymbol{F}^{ext}\left(\boldsymbol{x}_{ij}^l,t\right),\quad \boldsymbol{x}_{ij}^l\in\Gamma_s. \tag{6}$$

So for the ith particle with N boundary nodes, the total force $\boldsymbol{F}_i$ and the torque $\boldsymbol{T}_i$ on this particle are given by

$$\boldsymbol{F}_i(t)=\sum_{j=1}^{N}\boldsymbol{F}\left(\boldsymbol{x}_{ij}^l,t\right), \tag{7}$$

and

$$\boldsymbol{T}_i(t)=\sum_{j=1}^{N}\left(\boldsymbol{x}_{ij}^l-\boldsymbol{x}_i^{lc}\right)\times\boldsymbol{F}\left(\boldsymbol{x}_{ij}^l,t\right), \tag{8}$$

respectively, where $\boldsymbol{x}_i^{lc}$ is the center of gravity of the particle i.

The Newtonian dynamics equations for the ith particle are given by

$$\left.\begin{aligned}&M_i\tfrac{\mathrm{d}\boldsymbol{U}_i}{\mathrm{d}t}=\boldsymbol{F}_i,\\&\boldsymbol{I}_i\tfrac{\mathrm{d}\boldsymbol{\Omega}_i}{\mathrm{d}t}+\boldsymbol{\Omega}_i\times(\boldsymbol{I}_i\cdot\boldsymbol{\Omega}_i)=\boldsymbol{T}_i,\end{aligned}\right\} \tag{9}$$

where M_i and $\boldsymbol{I}_i$ are the mass and the inertial tensor of the ith particle; the translate velocity, $\boldsymbol{U}_i$, and angular velocity, $\boldsymbol{\Omega}_i$, can be computed by numerical solution of Eq. (9).

2.2. Lattice Boltzmann method with external boundary force

The lattice Boltzmann equation is often written as (Aidun et al., 1998; Chen et al., 1992; Hou et al., 1995; Mcnamara and Zanetti, 1988; Qian et al., 1992)

$$f_k(\boldsymbol{x}^e+\boldsymbol{e}_k,t+1)=f_k(\boldsymbol{x}^e,t)+\frac{1}{\tau}\left[f_k^{eq}(\boldsymbol{x}^e,t)-f_k(\boldsymbol{x}^e,t)\right]. \tag{10}$$

Here $f_k(\boldsymbol{x}^e,t)$ is the distribution function at $\boldsymbol{x}^e$ at time t, $f_k^{eq}(\boldsymbol{x}^e,t)$ is the equilibrium distribution function, τ is the single relaxation time constant and $\boldsymbol{e}_k$ is the discrete velocity vector. The fluid density ρ and the macroscopic fluid velocity $\boldsymbol{u}(\boldsymbol{x}^e,t)$ are given by

$$\rho(\boldsymbol{x}^e,t)=\sum_k f_k(\boldsymbol{x}^e,t)\quad\text{and}\quad\rho(\boldsymbol{x}^e,t)\boldsymbol{u}(\boldsymbol{x}^e,t)=\sum_k f_k(\boldsymbol{x}^e,t)\boldsymbol{e}_k. \tag{11}$$

The most common lattice model for three-dimensional case is D3Q19, which uses cubic lattice with nineteen discrete velocity directions (Aidun et al., 1998) for the fluid particles moving along the horizontal, vertical and diagonal links. The equilibrium distribution function is defined as

$$f_k^{eq}=w_k\rho\left[1+3\boldsymbol{e}_k\cdot\boldsymbol{u}+\frac{9}{2}(\boldsymbol{e}_k\cdot\boldsymbol{u})^2-\frac{3}{2}|\boldsymbol{u}|^2\right], \tag{12}$$

with $w_0=1/3$, $w_{1-6}=1/18$ (non-diagonal directions), and $w_{7-18}=1/36$ (diagonal directions) in three-dimensional D3Q19 model. For the present model, the pseudo speed of sound is $c_s=\sqrt{1/3}$ and the kinematic viscosity is $\nu=(2\tau-1)/6$.

There are two independent but overlapping grid systems in EBF method. The fluid domain is represented by the Eulerian grid and each fiber is represented by a Lagrangian grid. The no-slip boundary condition is satisfied by the requirement that the fluid velocity is equal to the fiber velocity at the fiber boundary node. We have to emphasize here that the solid boundary in LBM with SBB and the LBM with EBF is different, as show in Fig. 1. In SBB the solid boundary is halfway between fluid and solid nodes, where in EBF, the solid boundary represented by the Lagrangian grid nodes is the actual and precise boundary of the particle moving continuously through the fluid domain.

By adding an additional term to the collision function, the fluid–solid interaction force $\boldsymbol{g}$ from Eq. (5) is included in the lattice Boltzmann equation as

$$f_k(\boldsymbol{x}^e+\boldsymbol{e}_k,t+1)=f_k(\boldsymbol{x}^e,t)+\frac{1}{\tau}\left[f_k^{eq}(\boldsymbol{x}^e,t)-f_k(\boldsymbol{x}^e,t)\right]+\frac{3}{2}w_k\boldsymbol{g}\cdot\boldsymbol{e}_k. \tag{13}$$

2.3. Flexible fiber model

The flexible fiber is modeled as a chain of N rods and $N+1$ hinges, as shown in Fig. 2. Each rod has an equilibrium length of l and diameter D. The fiber length is $L=Nl$, and fiber aspect ratio $r_p=L/D$. We use four boundary nodes on the circumference of each hinge to calculate the fluid–solid interaction force, as shown in Fig. 3. Rods bend, twist about the hinges and change the length due to the forces that are applied on the fiber boundary nodes. This model is used to calculate the fiber deformation by the real material properties such as Young's modulus and shear modulus.

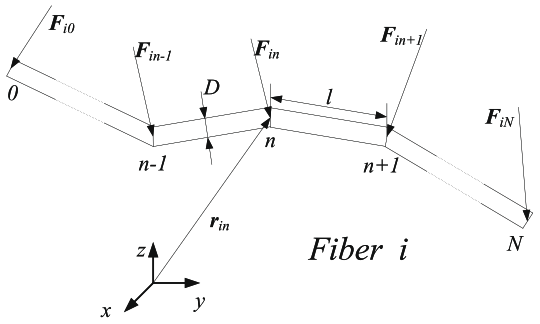

Fig. 2. The flexible fiber is modeled as a chain of rods.

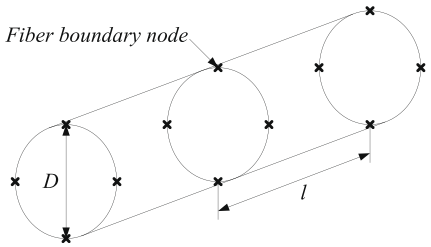

Fig. 3. The boundary nodes on the circumference of each hinge.

The assumptions are:

(i) The suspending fluid is incompressible Newtonian fluid and the bulk flow is assumed to be homogeneous, $\boldsymbol{U}^{\infty}(y) = \dot{\gamma} y$.
(ii) The fiber diameter and length are large enough so that the Brownian motion may be negligible.

The force densities applied on the fiber boundary nodes are the fluid–solid interaction force $\boldsymbol{F}^{fsi}$, the external force which could include the gravitational force $\boldsymbol{F}^{gra}$ and interparticle (electrical $\boldsymbol{F}^{ele}$, contact $\boldsymbol{F}^{con}$ or lubrication $\boldsymbol{F}^{lub}$) forces. The effective volume for each hinge is $dQ \equiv L\pi D^2/(4(N+1))$.

In this simulation, the densities of fluid and fiber are very close and the gravitational force is balanced by the buoyancy force and we only consider the lubrication force. A similar lubrication force used by Yamane et al. (1994, 2001) is also used here with an additional limitation for the case when actual contact of hinges occur. Let $\boldsymbol{V}_{in}$ and $\boldsymbol{V}_{jm}$ be the velocity of hinge n in fiber i and hinge m in fiber j, respectively (note, i could be equal to j), $\boldsymbol{r}_{in-jm} \equiv \boldsymbol{r}_{in} - \boldsymbol{r}_{jm}$ is the position vector from hinge m to hinge n, and $|\boldsymbol{r}_{in-jm}|$ is the length of the vector. The relative velocity component $\boldsymbol{V}^{lub}_{in-jm}$ between these hinges is

$$\boldsymbol{V}^{lub}_{in-jm} = \frac{\boldsymbol{r}_{in-jm}}{|\boldsymbol{r}_{in-jm}|}\left[\frac{\boldsymbol{r}_{in-jm}}{|\boldsymbol{r}_{in-jm}|}\cdot(\boldsymbol{V}_{in} - \boldsymbol{V}_{jm})\right]. \tag{14}$$

The lubrication force density between hinge in and jm is given by

$$\boldsymbol{F}^{lub}_{in-jm} = -\frac{9\mu \boldsymbol{V}^{lub}_{in-jm}}{2D(|\boldsymbol{r}_{in-jm}| - D)}. \tag{15}$$

Then the lubrication force density applied on hinge in is

$$\boldsymbol{F}^{lub}_{in} = \sum_{jm} \boldsymbol{F}^{lub}_{in-jm}. \tag{16}$$

To avoid fibers cross each other and to remove singularities when overlapping of hinges occurs ($|\boldsymbol{r}_{in-jm}| - D = 0$), the use of Eq. (15) is restricted in the range of $D + \epsilon \leqslant |\boldsymbol{r}_{in-jm}| \leqslant 1.25D$, where ϵ is a very small positive number to ensure a stable numerical simulation. If the gap is smaller than ϵ, the translation and rotation velocities are reset to make sure the relative velocity component along the direction with minimum distance between the surfaces is equal to zero.

The fluid–solid interaction force $\boldsymbol{F}^{fsi}_{in}$ is given by Eq. (4), the total force density imposed on hinge in is

$$\boldsymbol{F}_{in} = \boldsymbol{F}^{fsi}_{in} + \boldsymbol{F}^{lub}_{in}, \tag{17}$$

and the total force density applied on fiber i is $\boldsymbol{F}_i = \sum_{n=0}^{N} \boldsymbol{F}_{in}$.

The total force density on each hinge can be split into two parts, $\boldsymbol{F}^{mov}_{in}$ causes acceleration and $\boldsymbol{F}^{def}_{in}$ causes fiber bending, twisting and rotation. From this definition,

$$\boldsymbol{F}^{mov}_{in} = \boldsymbol{F}_i/(N+1) \quad \text{and} \quad \boldsymbol{F}^{def}_{in} = \boldsymbol{F}_{in} - \boldsymbol{F}^{mov}_{in}. \tag{18}$$

It is clear that $\sum_n \boldsymbol{F}^{mov}_{in} = \boldsymbol{F}_i$ and $\sum_n \boldsymbol{F}^{def}_{in} = 0$. The change of the length of rod in (the rod between hinge $in-1$ and in), dl_{in} is

$$dl_{in} = \frac{l}{E_Y(\pi D^2/4)}\left[\boldsymbol{p}_{in}\cdot\left(\boldsymbol{F}^{def}_{in} - \boldsymbol{F}^{def}_{in-1}\right)\right]dQ. \tag{19}$$

Here E_Y is the Young's modulus of the fiber, $\boldsymbol{p}_{in}$ is the unit vector parallel to the axis of symmetry of rod in and

$$\boldsymbol{p}_{in} = \frac{\boldsymbol{r}_{in} - \boldsymbol{r}_{in-1}}{|\boldsymbol{r}_{in} - \boldsymbol{r}_{in-1}|}. \tag{20}$$

Once the forces are known, the moments acting at each hinge can be calculated. For hinge n in fiber i, the moment that causing flexure is

$$\boldsymbol{Y}_{in} = \sum_{m=n+1}^{N}(\boldsymbol{r}_{im} - \boldsymbol{r}_{in}) \times \boldsymbol{F}^{def}_{im}\,dQ - \sum_{m=0}^{n-1}(\boldsymbol{r}_{im} - \boldsymbol{r}_{in}) \times \boldsymbol{F}^{def}_{im}\,dQ. \tag{21}$$

This moment can be decomposed into bending and twisting vector components, $\boldsymbol{Y}^{b}_{in}$ and $\boldsymbol{Y}^{t}_{in}$ respectively. The twisting moment is given by

$$\boldsymbol{Y}^{t}_{in} = \boldsymbol{p}_{in}(\boldsymbol{p}_{in}\cdot\boldsymbol{Y}_{in}), \tag{22}$$

and the bending moment

$$\boldsymbol{Y}^{b}_{in} = \boldsymbol{Y}_{in} - \boldsymbol{Y}^{t}_{in}. \tag{23}$$

The bending and twisting angles (β_{in} and α_{in}) can be calculated as

$$\begin{aligned} |\boldsymbol{Y}^{b}_{in}| &= -(\beta_{in} - \beta^{eq}_{in})E_Y I/l, \\ |\boldsymbol{Y}^{t}_{in}| &= -(\alpha_{in} - \alpha^{eq}_{in})E_G J/l. \end{aligned} \tag{24}$$

Here E_G is the shear modulus of the fiber material, I and J are the appropriate area moments of inertia. For a circular cylinder with diameter D, $I = \pi D^4/64$ and $J = \pi D^4/32$. The angles β^{eq}_{in} and α^{eq}_{in} are specified to mimic different equilibrium fiber shapes. For an intrinsically straight fiber, $\beta^{eq}_{in} = 0$ and $\alpha^{eq}_{in} = 0$.

The computational algorithm used in the LBM–EBF method can be summarized as follows:

(i) At $t = t_0$, the initial fluid velocity in the fluid domain and the fiber velocity, position and orientation are known.
(ii) The fluid velocity $\boldsymbol{U}_f$ on the boundary node is obtained by Eq. (2), the fluid–solid interaction force $\boldsymbol{F}^{fsi}$ is calculated from Eq. (4) and the lubrication force is updated by Eq. (16). Both forces are applied on the fiber boundary nodes.
(iii) The total force and torque acting on the fiber are calculated according to Eqs. (7) and (8); the fiber velocity, position and orientation are updated by numerical integration, and the fiber deformation is calculated by the flexible fiber model.
(iv) The fluid–solid interaction force also acting back on the fluid lattice nodes are computed by Eq. (5) and the fluid field is solved by the modified LBM Eq. (13). The computations loop back to step (ii).

3. Sample problems

In this section we provide some example problems to validate the LBM–EBF method for flexible fiber simulation. In the next Section 3.1, we examine the accuracy of computing the shear stress on the surface of a rotating cylinder at different aspect ratios r_p. In Section 3.2, we simulate the flexible fiber with different stiffness in simple shear flow where the orbits of bent fiber are compared with experimental data from Forgacs and Mason (1959). Comparison of computational results for rigid fiber suspensions with experiments is presented in Section 3.3. Computational simula-

tions of flexible fiber suspensions and the effect of fiber stiffness on relative viscosity are discussed in Section 3.4.

To improve the computational efficiency and remove wall effects, an unbounded shear domain is implemented based on the Lees–Edwards boundary condition (LEBC) (Lees and Edwards, 1972) as described by Wagner and Pagonabarraga (2002) and MacMeccan et al. (2009). The uniform shear flow has been reached without the moving solid walls, the spatial inhomogeneities that are introduced by the wall effects are eliminated and the bulk rheological properties can be recovered on smaller fluid domain with fewer particles. Periodic boundary conditions are applied in the flow and vorticity directions (x and z directions in Fig. 4, respectively).

3.1. Single rigid fiber

Bretherton (1962) expanded Jeffery's solution (Jeffery, 1922) to any axisymmetric particle and used an effective aspect ratio r_e equal to r_p for an ellipsoidal particle. For a single ellipsoidal particle in Stokes shear flow, the governing equations are given by (Jeffery, 1922)

$$\dot{\phi} = \frac{\dot{\gamma}\left(r_e^2\cos^2\phi + \sin^2\phi\right)}{\left(r_e^2+1\right)}, \tag{25}$$

and

$$\dot{\theta} = \frac{\dot{\gamma}(r_e^2-1)\cos\phi\sin\phi\cos\theta\sin\theta}{\left(r_e^2+1\right)}. \tag{26}$$

Here $\dot{\gamma}$ is the shear rate, ϕ and θ are the orientation angles in the spherical coordinate system, as shown in Fig. 4; x, y and z coordinates are in the flow direction, velocity gradient direction and vorticity axis direction, respectively.

Integrating Eqs. (25) and (26) yield

$$\tan\phi = r_e\tan\left(\frac{2\pi t}{T_p}+\phi_0\right), \tag{27}$$

and

$$\tan\theta = \frac{C_j r_e}{\left(r_e^2\cos^2\phi+\sin^2\phi\right)^{1/2}}, \tag{28}$$

respectively, where C_j and ϕ_0 are respectively referred to as the Jeffery's orbit constant and phase angle. The particle rotation period T_p increases with increasing ellipsoid aspect ratio, $\dot{\gamma}T_p = 2\pi(r_e + 1/r_e)$. For a rigid cylinder of aspect ratio $r_p = L/D$, the equivalent aspect ratio has been measured by Trevelyan and Mason (1951). The computational results presented in Fig. 5 shows agreement with Cox's solution (Cox, 1971), $r_e = 1.24r_p/\sqrt{\ln r_p}$, and the experimental data of Trevelyan and Mason (1951). In our simulation, the computational domain is $100\times100\times10$ lattice nodes and the suspending fibers have diameter of $D = 0.2$ LBM unit lattice size. This demonstrates that the no-slip boundary condition on the ellipsoid surface is satisfied.

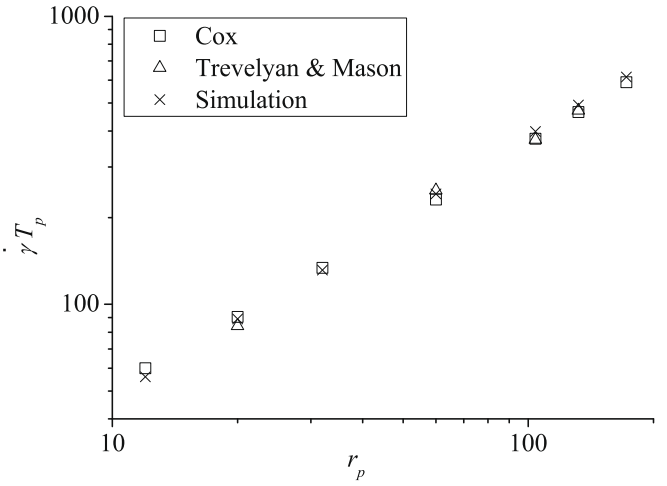

Fig. 5. Non-dimensional rotation period $\dot{\gamma}T_p$ *vs.* fiber aspect ratio r_p in a x, y simple shear flow.

To show the accuracy of the interpolation in EBF method, especially for fibers that have sub-grid diameters, several simulations were performed for fibers with diameter $D = 1$, 0.4, 0.1 and 0.04 lattice units with fixed aspect ratio, $r_p = 32$. In these simulations, only the size of the LBM lattice unit is changed where all other parameters remain the same. For example, the size of the LBM lattice unit for $D = 0.1$ is ten times larger than the case $D = 1$. As shown in Fig. 6, results show very small deviation between each other and show good agreement with Cox's model with less than 2% difference.

3.2. Single flexible fiber

To quantitatively measure the bending deformation of a single flexible fiber, Forgacs and Mason (1959) took photographs at short time intervals during the rotation of a long Nylon filament ($r_p = 170$). The result presented in Fig. 7 clearly shows the increase in deformation with shear rate, $\dot{\gamma}$. It also shows the asymmetry of the loci about the y axis due to the compression and the extension

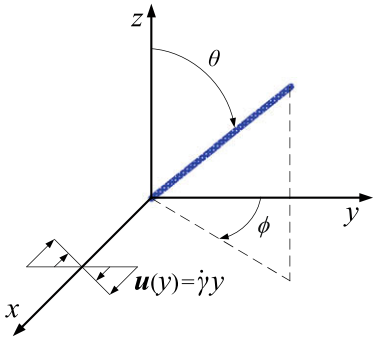

Fig. 4. The spherical coordinate system for a fiber in a x, y simple shear flow.

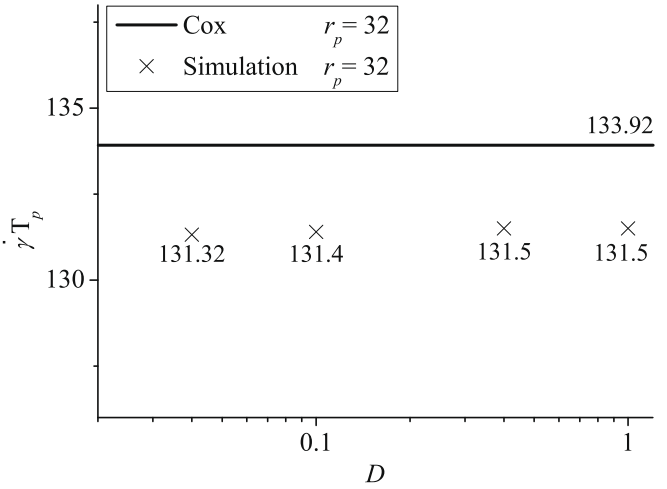

Fig. 6. Non-dimensional rotation period $\dot{\gamma}T_p$ *vs.* fiber diameter D.

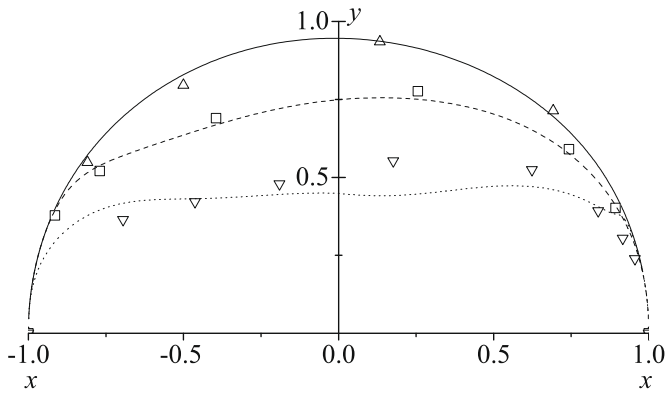

Fig. 7. Polar plot of the loci of the end of a Nylon filament ($r_p = 170$) during rotation in a x, y simple shear flow. The open triangles (△), open squares (□) and open upside-down triangles (▽) are the experiment data of Forgacs and Mason (1959) for shear rate $\dot{\gamma} = 3.20,\ 3.54$ and $4.25\ s^{-1}$. The solid line (—), dash line (- - -) and dot line (···) are the corresponding simulation results.

forces. To reproduce the existing experimental results, the fiber and the suspending fluid have the same physical properties as Forgacs and Mason used in the experiment; the suspending fibers have diameter of $D = 0.0122$ mm, aspect ratio $r_p = 170$ and Young's modulus $E_Y = 6.3$ GPa. The dynamic viscosity of the suspending fluid is $\mu = 9.12$ Pa s. In our simulation, the computational domain is $100 \times 100 \times 10$ lattice nodes and the suspending fibers have diameter of $D = 0.2$ LBM unit lattice size. The simulation result is in fairly good agreement with the experimental result in Fig. 7.

3.3. Rigid fiber suspensions

One of the main objectives of our work is to obtain a better understanding of the rheological behavior of flexible fiber suspensions. Experimental results are often presented in terms of relative shear viscosity, defined as

$$\eta \equiv \frac{\mu_{eff}}{\mu}, \tag{29}$$

where μ is the viscosity of the suspending fluid, and μ_{eff} is the effective shear viscosity, given by

$$\mu_{eff} = \frac{\Sigma_{xy}}{2E_{xy}}, \tag{30}$$

where $E_{xy} = \dot{\gamma}/2$ is the shear strain component of the strain rate tensor, $\boldsymbol{E}$, and Σ_{xy} is the shear stress component of the stress tensor $\boldsymbol{\Sigma}$.

Blakeney (1966) used a Couette device to measure the viscosity of rigid fiber suspensions in a Newtonian fluid. We compare the relative shear viscosity computed from our simulations with his experimental results. In our simulation, the computational domain is $80 \times 80 \times 80$ lattice nodes and the suspending fibers have diameter of $D = 0.8$ LBM unit lattice size. The length and aspect ratio of a fiber is $L = 16$ LBM unit lattice size and $r_p = 20$ respectively. As shown in Fig. 8, the trend of the computational result follows experimental data well. The simulations seem to have small overprediction.

3.4. Flexible fiber suspensions

Fiber stiffness plays an important role in fiber suspension microstructure and rheology. Forgacs and Mason (1959) and Goldsmith and Mason (1967) have studied the flow induced deformation of a single flexible fiber in simple shear flow. A cylindrical

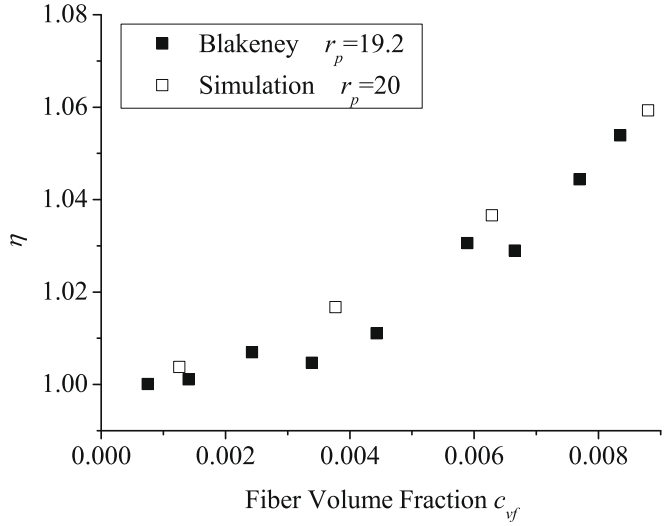

Fig. 8. The relative shear viscosity η *vs.* fiber volume fraction c_{vf} in dilute regime. The solid squares (■) are the experiment data of Blakeney (1966), the open squares (□) are the results from present LBM with EBF.

flexible fiber is predicted to bend when the non-dimensional parameter bending ratio, given by

$$BR \equiv \frac{E_Y(\ln 2r_e - 1.5)}{2(\mu\dot{\gamma})r_p^4}, \tag{31}$$

is small. There has been experiments to measure the viscosity of flexible fiber suspensions (Bibbo, 1987). In Bibbo's experiment, the nylon fiber has density of $\rho_f = 1.25 \times 10^3\ kg/m^3$, diameter of $D = 0.12$ mm and Young's modulus $E_Y = 3.0$ GPa. The suspending fluid has density $\rho = 0.97 \times 10^3\ kg/m^3$ and dynamic viscosity $\mu = 13$ Pa s. The flexible fiber suspensions are simulated with volume fraction $1.7\% \leqslant c_{vf} \leqslant 12.4\%$, corresponding to the number of fibers between 180 and 1260. The bending ratio corresponding to aspect ratios $r_p = 16$, 32 and 52 are $BR = 2942$, 248 and 42 respectively. In our simulation, the computational domain is $80 \times 120 \times 80$ lattice nodes and the suspending fibers have diameter of $D = 0.4$ LBM unit lattice size. As shown in Fig. 9, the simula-

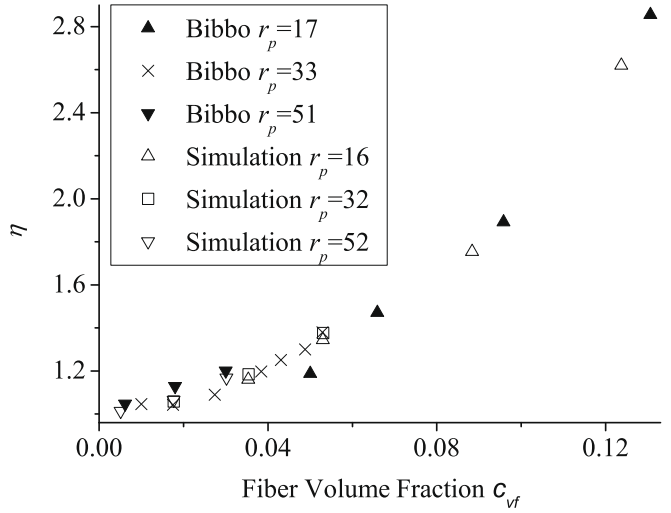

Fig. 9. The relative shear viscosity η *vs.* fiber volume fraction c_{vf} for fibers with different aspect ratio. The solid triangles (▲), crosses (×) and solid upside-down triangles (▼) are the experiment data of Bibbo (1987), the open triangles (△), open squares (□) and open upside-down triangles (▽) are the results from present LBM with EBF.

tion results compare well with experimental results in the range of fiber aspect ratio and volume fraction covered by the experiments. The effect of aspect ratio at a given volume fraction on η seems to be relatively small.

To examine the effect of bending ratio on relative viscosity, we simulate a case with aspect ratio $r_p = 16$. Fig. 10 shows the relation between the relative shear viscosity η and the bending ratio BR in an unbounded shear flow. For this example, the number of fibers is 540, fiber volume fraction $c_{vf} = 0.053$, fiber Young's modulus covers the range $0.15\ \text{MPa} \leqslant E_Y \leqslant 3 \times 10^3\ \text{MPa}$ with corresponding bending ratio in the range $0.147 \leqslant BR \leqslant 2942$. The suspending fluid has density $\rho = 0.97 \times 10^3\ \text{kg/m}^3$ and dynamic viscosity $\mu = 13$ Pa s. These simulations show that decrease in bending ratio BR (more deformable fiber) leads to increase of the relative shear viscosity η.

One can explain this effect by considering the impact of bending ratio on fiber orientation distribution. It is well known that the fiber orientation distribution has strong effect on the suspension shear viscosity. Batchelor (1971) derived the stress tensor of freely moving, non-Brownian, rigid fiber suspensions, given by

$$\boldsymbol{\Sigma} = 2\mu\boldsymbol{E} + \mu_{fiber}\left(\langle \boldsymbol{pppp}\rangle - \frac{1}{3}\boldsymbol{I}_n\langle \boldsymbol{pp}\rangle\right) : \boldsymbol{E}, \tag{32}$$

where $\boldsymbol{E}$ is the strain rate tensor, $\boldsymbol{I}_n$ is the unit tensor. μ_{fiber} is a function of fiber concentration, orientation distribution and fiber aspect ratio. The shear viscosity, μ_{Ba}, can be derived from Eq. (32) to be

$$\mu_{Ba} = \mu + \mu_{fiber}\left\langle p_x^2 p_y^2\right\rangle, \tag{33}$$

where $\boldsymbol{p} = p_x\boldsymbol{e_x} + p_y\boldsymbol{e_y} + p_z\boldsymbol{e_z}$ is a unit vector parallel to the fiber axis of symmetry, and $\boldsymbol{e_x}$, $\boldsymbol{e_y}$ and $\boldsymbol{e_z}$ are the unit vectors in the flow direction, velocity gradient direction and vorticity axis direction, respectively. $\langle\rangle$ denotes average over all fibers in the suspension. From Eq. (33), it is clear that the fiber orientation has strong effect on the suspension shear viscosity. The shear stress has the maximum value when fiber orientation angle ϕ is equal to $\pi/4$ or $3\pi/4$ and has the minimum value when ϕ equal to 0, $\pi/2$ or π. Fig. 11 shows the ϕ distribution with different bending ratio BR for the same cases depicted in Fig. 10. For increasing bending ratio (more rigid fiber), the ϕ distribution becomes narrower showing 'longer-time' orientation in the vicinity of the x–z plane, thus reducing the suspension shear viscosity. A small asymmetry of the ϕ distribution was observed in the small BR regime, indicating that fiber–fiber interaction and fiber deformation are present at $BR < 3$.

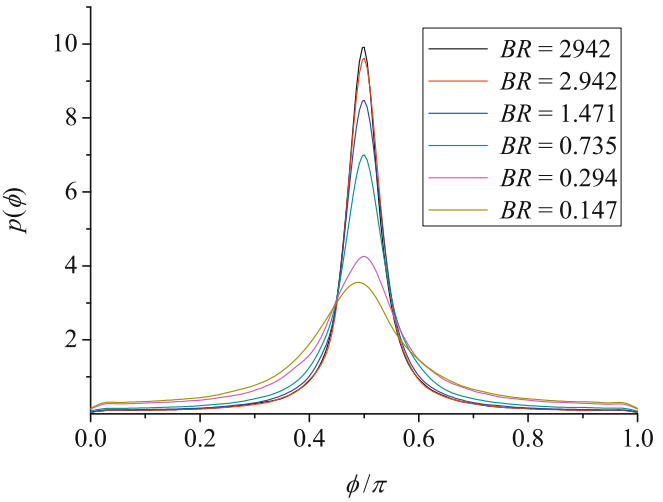

Fig. 11. The ϕ distribution for different Bending ratio BR. Fiber aspect ratio $r_p = 16$, volume fraction $c_{vf} = 0.053$.

In Fig. 12, the average number of contact points per fiber $\langle n_c\rangle$ is plotted as a function of the bending ratio BR for the same cases depicted in Fig. 10. Mean values were taken for $p(\phi)$ and $\langle n_c\rangle$, by time averaging after preconditioning. The decrease of the bending ratio BR leads to the increase of $\langle n_c\rangle$. As $\langle n_c\rangle$ increases, fibers interact more frequently with increased contribution to the shear stress. A more thorough investigation of the effects of fiber stiffness on the rheology of fiber suspensions is in progress.

4. Conclusions

We have presented the LBM with external boundary force method for direct simulation of flexible fibers in Newtonian suspension. Application to the lattice Boltzmann method provides an efficient and more stable computational tool compared to the conventional LBM with SBB. The operations in LBM with EBF are local, it can be easily programmed for parallel machines. The method has been validated by comparing the 3D computational results with experimental results and theoretical solutions. The

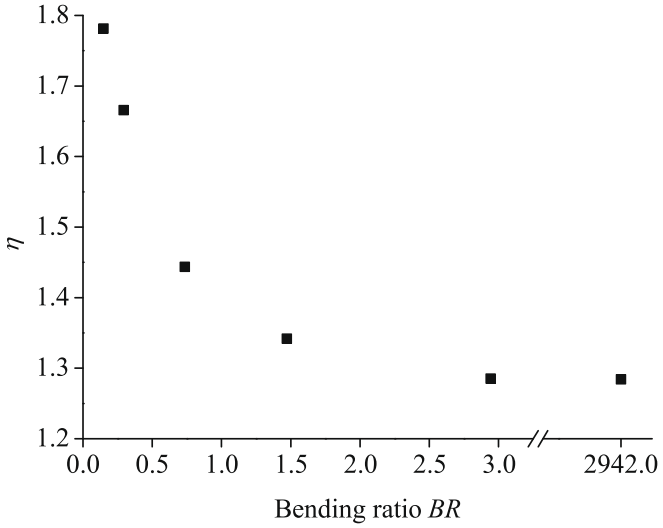

Fig. 10. The relative shear viscosity η *vs.* Bending ratio BR. Fiber aspect ratio $r_p = 16$, volume fraction $c_{vf} = 0.053$.

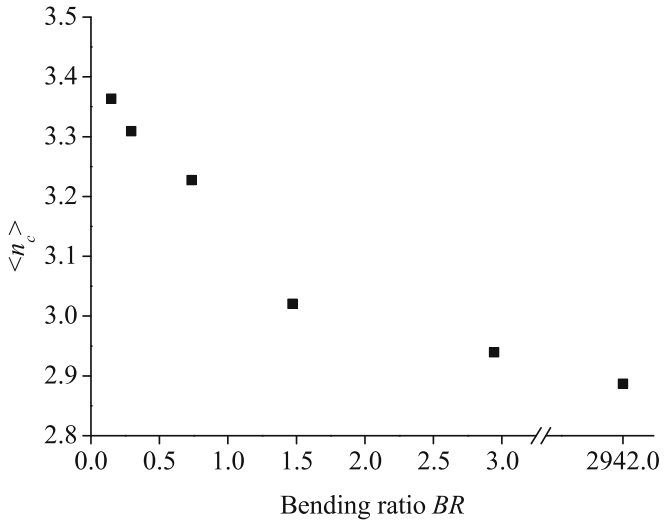

Fig. 12. The average number of contact points per fiber $\langle n_c\rangle$ *vs.* Bending ratio BR. Fiber aspect ratio $r_p = 16$, volume fraction $c_{vf} = 0.053$.

simulations seem to slightly overpredict the shear viscosity in the dilute regime as compared to Blakeney (1966)'s data. This could be due to the unbounded periodic shear layer used in the simulations as compared with the wall-bounded experimental results. This effect may result in the small discrepancy in the magnitude of relative viscosity in the dilute regime. However, in the case of higher volume fraction suspension flow, considered in Fig. 9, the magnitude of relative viscosity is much higher masking the small deviations between the experimental and computational results.

The bending ratio of the fiber used in Blakeney's experiments is very large (i.e., $BR \sim 4 \times 10^4$). Therefore, in simulations, we use a rigid fiber. We have shown that the fiber bending ratio has significant influence on the flow rheology in the range $BR < 3$, where for $BR > 3$, the fiber can be considered to be rigid. It is clear that the influence of fiber bending ratio on the fiber orientation distribution, shown in Fig. 11, is a major contributor to the variation in relative viscosity presented in Fig. 10. More complete details on the underlying physics will be reported upon completion of the work in progress.

References

Aidun, C.K., Lu, Y., 1995. Lattice-Boltzmann simulation of solid particles suspended in fluid. J. Stat. Phys. 81, 49–61.

Aidun, C.K., Lu, Y., Ding, E., 1998. Direct analysis of particulate suspensions with inertia using the discrete Boltzmann equation. J. Fluid Mech. 373, 287.

Anczurowski, E., Mason, S.G., 1967. The kinetics of following dispersions. J. Colloid Interface Sci. 23, 533.

Batchelor, G.K., 1970. Slender-body theory for particles of arbitrary cross-section in stokes flow. J. Fluid Mech. 44, 419.

Batchelor, G.K., 1971. The stress generated in a non-dilute suspensions of elongated particles by pure straining motion. J. Fluid Mech. 46, 813.

Bibbo, M., 1987. Rheology of semi-concentrated fiber suspensions. Ph.D. Thesis, Massachusetts Institute of Technology.

Blakeney, W., 1966. The viscosity of suspensions of straight, rigid rods. J. Colloid Interface Sci. 22, 324.

Bouzidi, M., Firdaouss, M., Lallemand, P., 2001. Momentum transfer of a Boltzmann-lattice fluid with boundaries. Phys. Fluids 13, 3452.

Bretherton, F.P., 1962. Slow motion round a cylinder in a simple shear. J. Fluid Mech. 12, 591.

Buick, J.M., Greated, C.A., 2000. Gravity in a lattice Boltzmann model. Phys. Rev. E 61, 5307.

Chen, H., Chen, S., Matthaeus, W.H., 1992. Recovery of the navier-stokes equations using a lattice-gas Boltzmann method. Phys. Rev. A 45, 5339.

Chun, B., Ladd, A.J.C., 2007. Interpolated boundary condition for lattice Boltzmann simulations of flows in narrow gaps. Phys. Rev. E 75, 066705.

Claeys, I.L., Brady, J.F., 1993. Suspensions of prolate spheroids in stokes flow. Part 1. Dynamics of a finite number of particles in an unbounded fluid. J. Fluid Mech. 251, 411.

Clausen, J.R., Aidun, C.K., 2009. Galilean invariance in the lattice-Boltzmann method and its effect on the calculation of rheological properties in suspensions. Int. J. Multiphase Flow 35, 307.

Cox, R.G., 1971. The motion of long slender bodies in a viscous fluid. 2. Shear flow. J. Fluid Mech. 45, 625–657.

Ding, E., Aidun, C.K., 2003. Extension of the lattice-Boltzmann method for direct simulation of suspended particles near contact. J. Stat. Phys. 112, 685–708.

Dinh, S., Armstrong, R., 1984. A rheological equation of state for semi-concentrated fiber suspensions. J. Rheol. 28, 207.

Doi, M., Edwards, S.F., 1978a. Dynamics of concentrated polymer systems i; Brownian motion in equilibrium state. J. Chem. Soc. Faraday Trans. II 74, 1789.

Doi, M., Edwards, S.F., 1978b. Dynamics of concentrated polymer systems ii; molecular motion under flow. J. Chem. Soc. Faraday Trans. II 74, 1802.

Einstein, A., 1906. A new determination of the molecular dimensions. Ann. Phys. 19, 289.

Folgar, F., Tucker, C.L., 1984. Orientation behavior of fibers in concentrated suspensions. J. Reinf. Plastic Compos. 3, 98.

Forgacs, O.L., Mason, S.G., 1959. Particle motions in sheared suspensions. 9. Spin and deformation of thread-like particles. J. Colloid Interface Sci. 14, 457.

Ginzburg, I., d'Humieres, D., 2003. Multireflection boundary conditions for lattice Boltzmann models. Phys. Rev. E 68, 066614.

Goldsmith, H.L., Mason, S.G., 1967. The microrheology of dispersions. Rheology 4, 85–201.

Goldstein, D., Handler, R., Sirovich, L., 1993. Modeling a no-slip flow boundary with an external force field. J. Comput. Phys. 105, 354–366.

Goto, S., Nagazono, H., Kato, H., 1986. The flow behavior of fiber suspensions in newtonian fluids and polymer solutions. I: mechanical properties. Rheol. Acta 25, 119.

Guo, Z., Zheng, C., Shi, B., 2002. Discrete lattice effects on the forcing term in the lattice Boltzmann method. Phys. Rev. E 65, 046308.

He, X., Zou, Q., Luo, L.S., Dembo, M., 1997. Analytic solutions and analysis on non-slip boundary condition for the lattice Boltzmann BGK model. J. Stat. Phys. 87, 115.

Hinch, E.J., Leal, L.G., 1972. The effect of Brownian motion on the rheological properties of a suspension of non-spherical particles. J. Fluid Mech. 52, 683.

Hou, S., Zou, Q., Chen, S., Doolen, G., Cogley, A.C., 1995. Simulation of cavity flow by lattice Boltzmann method. J. Comput. Phys. 118, 329.

Jeffery, G.B., 1922. The motion of ellipsoidal particles immersed in a viscous fluid. Proc. Roy. Soc. Lond. Ser. A 102, 161.

Joung, C.G., Phan-Thien, N., Fan, X.J., 2001. Direct simulation of flexible fibers. J. Non-Newton. Fluid Mech. 99, 1.

Ladd, A.J.C., 1994. Numerical simulations of particulate suspensions via a discretized Boltzmann equation. Part 1. Theoretical foundation. J. Fluid Mech. 271, 285.

Ladd, A.J.C., Verberg, R., 2001. Lattice-Boltzmann simulation of particle-fluid suspensions. J. Stat. Phys. 104, 1191.

Lee, W.I., Springer, G.S., 1982. The motion of slender particles in shear flow. J. Reinf. Plastics Compos. 1, 279.

Lees, A.W., Edwards, S.F., 1972. The computer study of transport processes under extreme conditions. J. Phys. C 5, 1921.

Liboff, R., 2003. Kinetic Theory: Classical, Quantum, and Relativistic Descriptions, 3rd ed. Springer.

Lindstrom, S.B., Uesaka, T., 2008. Simulation of semidilute suspensions of non-Brownian fibers in shear flow. J. Chem. Phys. 128, 024901.

MacMeccan, R.M., Clausen, J.R., Neitzel, G.P., Aidun, C.K., 2009. Simulating deformable particle suspensions using a coupled lattice-Boltzmann and finite-element method. J. Fluid Mech. 618, 13.

Martys, N.S., Shan, X., Chen, H., 1998. Evaluation of the external force term in the discrete Boltzmann equation. Phys. Rev. E 58, 6855.

Mcnamara, G.R., Zanetti, G., 1988. Use of the Boltzmann equation to simulate lattice-gas automata. Phys. Rev. Lett. 61, 2332.

Okagawa, A., Mason, S.G., 1973. The kinetics of flowing dispersions VII. Oscillatory behavior of rods and discs in shear flow. J. Colloid Interface Sci. 45, 330.

Peskin, C.S., 2002. The immersed boundary method. Acta Numer. 11, 479.

Qi, D., 2006. A new method for direct simulations of flexible filament suspensions in non-zero reynolds number flows. Int. J. Numer. Methods Fluids 54, 103.

Qian, Y., D'Humieres, D., Lallemand, P., 1992. Lattice BGK models for Navier–Stokes equation. Europhys. Lett. 17, 479.

Rezak, S., 2008. Analysis of flexible fiber suspensions using the lattice Boltzmann method. Ph.D. Thesis, Georgia Institute of Technology.

Ross, R.F., Klingenberg, D.J., 1997. Dynamic simulation of flexible fibers composed of linked rigid bodies. J. Chem. Phys. 106, 2949.

Schmid, C.F., Switzer, L.H., Klingenberg, D.J., 2000. Simulation of fiber flocculation: effects of fiber properties and interfiber friction. J. Rheol. 44, 781.

Shaqfeh, E.S.G., Koch, D.L., 1988. The effect of hydrodynamic interactions on the orientation of axisymmetric particles flowing through a fixed bed of spheres or fibers. Phys. Fluids 31, 728.

Shaqfeh, E.S.G., Koch, D.L., 1990. Orientational dispersion of fibers in extensional flows. Phys. Fluids A 2, 1077.

Stover, C.A., Koch, D.L., Cohen, C., 1992. Observations of fiber orientation in simple shear flow of semi-dilute suspensions. J. Fluid Mech. 238, 277.

Trevelyan, B.G., Mason, S.G., 1951. Particle motions in sheared suspensions. 1. Rotations. J. Colloid Sci. 6, 354.

Wagner, A., Pagonabarraga, I., 2002. Lees-edwards boundary conditions for lattice Boltzmann. J. Stat. Phys. 107, 521.

Wu, J., Aidun, C.K., 2009. Simulating 3D deformable particle suspensions using lattice Boltzmann method with discrete external boundary force. International Journal for Numerical Method in Fluids, doi: 10.1002/fld.2043.

Yamamoto, S., Matsuoka, T., 1992. A method for dynamic simulation of rigid and flexible fibers in a flow field. J. Chem. Phys. 98, 644.

Yamane, Y., Kaneda, Y., Doi, M., 1994. Numerical simulation of semi-dilute suspensions of rodlike particles in shear flow. J. Non-Newton. Fluid Mech. 54, 405.